Atmospheric Research 262 (2021) 105801

Contents lists available at ScienceDirect

Atmospheric Research

journal homepage: www.elsevier.com/locate/atmosres

Precipitation over semi-arid regions of North Hemisphere affected by Atlantic Multidecadal Oscillation

Kaiwei Zhu [a], Xiaodan Guan [a,b,*], Jianping Huang [a,b], Jiamin Wang [a], Shuyang Guo [a], Chenyu Cao [a]

[a] Key Laboratory for Semi-Arid Climate Change of the Ministry of Education, College of Atmospheric Sciences, Lanzhou University, Lanzhou, China
[b] Collaborative Innovation Center for Western Ecological Safety, Lanzhou, China

ARTICLE INFO

Keywords:
Precipitation
Semi-arid regions
Atlantic Multidecadal Oscillation
Dynamic mechanism
Decadal variability

ABSTRACT

As a key variable in climate change over semi-arid regions, precipitation variation has received much attention from the public, but the local mechanisms involved are still not fully understood. The results presented in this study show as the Atlantic Multidecadal Oscillation (AMO) underwent a phase transition from the negative to a positive phase in the past 30 years, precipitation over the areas with annual precipitation below 400 mm decreased, while the areas with annual precipitation of more than 400 mm showed an increase of precipitation in the semi-arid regions. In the past two whole cycles of the AMO, during the positive phase, less precipitation was distributed in the semi-arid regions of North America, more precipitation in the semi-arid regions of North Africa, Iberian Peninsula, Asia Minor Peninsula, and India, while opposite change pattern was observed in the negative phase. Such precipitation patterns which depend on AMO are associated with the North Atlantic SST anomalies. In the positive phase of AMO, the elevated SST weakened the summer sea-level pressure over the Atlantic. Then, three cyclonic circulation anomalies appear over North Atlantic, North America, and eastern Pacific. The cyclonic circulation anomalies intersected over the semi-arid regions of North America and caused anomalous low-level divergence and the North Atlantic cyclonic circulation enhanced the African monsoon, even affecting the precipitation in the semi-arid regions around the Atlantic. In the negative phase, a roughly opposite flow field occurred. Besides, according to the prediction of the E3SM 1–1 model, the negative AMO will appear in the coming decade, the same AMO which contributed to the increased semi-arid precipitation over southern part of North America and the decreased semi-arid precipitation over North Africa.

1. Introduction

Although the linear change of global precipitation in recent years is near zero (Gu et al., 2007), regional precipitation has changed remarkedly due to redistribution of precipitation. More drought events and heavy rains caused by these regional variations are more severe in semi-arid areas (Dai, 2011; Kong et al., 2019). The definition of semi-arid area that is broadly accepted uses the ratio of annual precipitation (P) to potential evapotranspiration (PET). When the ratio, in terms of the aridity index (AI), is between one fifth and one half, the area is semi-arid (Feng and Fu, 2013; Huang et al., 2016; Middleton and Thomas, 1997; Scholes, 2020). Fig. S1 shows the drylands in the Northern Hemisphere (NH); clearly, the semi-arid regions ($0.2 < AI \leq 0.5$) are mainly located in western North America, North Africa, the Iberian Peninsula, and Central and East Asia. The semi-arid area is a transition zone between arid area and humid area (FAO, 1977; Gong et al., 2004; Huang et al., 2017; Miao et al., 2020), which has the characteristics of dry climate, lacking water resources, and fragile ecosystem; and it is sensitive to climate changes (Gong et al., 2004; Huang et al., 2019). In these regions, the extreme precipitation events are magnified and lead to severe disasters like landslide (Guan et al., 2019; Zhang and Wang, 2018).

Prior studies have revealed that the precipitation in the semi-arid areas is greatly influenced by oceanic oscillation factors on different time scales (Gao et al., 2017; Guan et al., 2019; Hu and Feng, 2012). For example, El Niño-Southern Oscillation (ENSO) and Pacific Decadal Oscillation (PDO) are the most representative interannual and interdecadal fluctuation of the climate system respectively (Mantua et al.,

* Corresponding author at: Key Laboratory for Semi-Arid Climate Change of the Ministry of Education, College of Atmospheric Sciences, Lanzhou University, Lanzhou, China.
E-mail address: guanxd@lzu.edu.cn (X. Guan).

https://doi.org/10.1016/j.atmosres.2021.105801
Received 8 April 2021; Received in revised form 3 August 2021; Accepted 3 August 2021
Available online 6 August 2021

1997; McPhaden et al., 2006). ENSO can modulate interannual precipitation variability (Chang et al., 2004; Ropelewski and Halpert, 1987) and PDO can exert decadal impact on precipitation by modifying atmosphere circulation (Kim et al., 2014; Mochizuki et al., 2010; Qian and Zhou, 2014). Moreover, precipitation variation is always a result of multifactorial effects (Kitzberger et al., 2007). For example, during the positive phase of the PDO, the ENSO's effects on North American summer precipitation are weakened and even vanished in some regions. Conversely, the effects of the ENSO are strengthened during the negative phase of the PDO (Hu et al., 2011). Even a single oceanic oscillation factor can dominantly impact precipitation variability at specific time scales. For the multidecadal precipitation variation, the Atlantic Multidecadal Oscillation (AMO) contributes a large proportion to the total variance (McCabe et al., 2004).

The AMO is the climate swing of sea surface temperature (SST) with a duration of 50–70 years (Kerr, 2000; Schlesinger and Ramankutty, 1994), which is defined as the weighted average of basin-scale SST anomalies in the North Atlantic (Enfield et al., 2001; Knight et al., 2006). As a near-global scale mode of observed multidecadal climate variability, the AMO has a great impact on global climate, including Sahel rainfall, Atlantic hurricanes and North American droughts (Guan et al., 2017; Knight et al., 2006; Ting et al., 2011; Wu et al., 2020; Wyatt et al., 2012). Here, we will focus on the multidecadal precipitation variation influenced by the AMO. Once we understand the connection between AMO and precipitation in semi-arid regions, such link will help long-term climate predictions, model evaluation, and government decision-making.

In this study, we examine the robustness and mechanism of the linkage between semi-arid regions' precipitation and AMO. This paper is arranged as follows. Methods and datasets used in this study are described in Section 2. In Section 3, the precipitation variation in semi-arid regions and its relationship with the AMO are presented, along with a mechanism at work. Finally, conclusions, discussion, and avenues for further study are presented in Section 4.

2. Methodology and data

2.1. Methodology

2.1.1. Ensemble empirical mode decomposition (EEMD) method

The EEMD is widely used to deal with nonlinear and non-stationary time series, like climate variables. This approach sifts an ensemble of white noise-added signal with a sufficient number of trials, and treats the mean as the final true result. The white noise will be averaged out in the process, and the rest are the components of the signal, which are true and physically meaningful (Wu and Huang, 2009). The decadal to multidecadal components of the AMO and regional precipitation indices are sifted from the filtered data by the EEMD in this study. We select the intrinsic mode functions (IMFs) that meet the requirements on the time scale, and add them up to obtain the signals we analyze. In the EEMD, an ensemble size of 400 is used, and the added white noise has a standard deviation of 0.2 (Luo et al., 2019).

2.2. Data

2.2.1. Precipitation, SST and AI data

In this study, we used gauge-based gridded precipitation dataset from the Global Precipitation Climatology Centre (GPCC) for the semi-arid land surface. The dataset has a spatial resolution of 0.5° by 0.5° and covers the period from 1891 to 2016 (https://opendata.dwd.de/climate_environment/GPCC/html/fulldata-monthly_v2018_doi_download.html). Based on the data from more than 79,000 stations, GPCC's new global precipitation climatology V.2018 is suitable for estimating inland precipitation (including most semi-arid regions) owing to much denser station network (Schneider et al., 2014). The precipitation in CRU TS v. 4.05 (Climatic Research Unit gridded Time Series Version 4.05) is used to checked the results from GPCC in this paper. It is a widely used dataset on a 0.5° latitude by 0.5° longitude grid and spans 1901–2018, which meets our needs for the long-time scale (Harris et al., 2020). The HadISST 1.1 monthly average SST data set is from Met Office Hadley Centre (https://www.metoffice.gov.uk/hadobs/hadisst/data/download.html), which has a spatial resolution of 1° by 1° and ranges from 1870 to present. The AI dataset used in this study is the same as that used in Huang et al. (2020), which has a spatial resolution of 0.5° by 0.5° and covers the period from 1948 to 2016.

2.2.2. AMO data

The AMO index is defined as the area-weighted average of monthly SST anomalies in the North Atlantic (Enfield et al., 2001). The index data covers the period from 1901 to the present (https://psl.noaa.gov/data/timeseries/AMO/). Since the main emphasis of the present study is the precipitation associated with the AMO on the multidecadal scale, the obtained AMO index is filtered by using an 11-year running average (Joshi and Ha, 2019). The same smoothing is also applied to the regional precipitation index. We chose the years when the AMO index is 0.5 standard deviation above the mean as the positive phase. Conversely, the years when the AMO index is 0.5 standard deviation below the mean are considered as the negative phase (Mo et al., 2009).

2.2.3. Reanalysis data

We use the sea-level pressure (SLP), geopotential height, omega, and wind fields to explain how the AMO modulates the precipitation in semi-arid regions. These fields are from the 20th Century Reanalysis V3 dataset, which have a spatial resolution of 1° by 1° over the period of 1836–2015 (https://psl.noaa.gov/data/gridded/data.20thC_ReanV3.html). The long-time range of this dataset allows us to examine the climate processes that are connected with the AMO at the multidecadal scale.

2.2.4. Model outputs

We selected 14 models (Table S1) participated in CMIP6, and only the first ensemble member from each CMIP6 model was used (Xie et al., 2019). The historical runs of these models were downloaded, which can serve as an important benchmark for assessing model performance through evaluation against observations (Eyring et al., 2016). In addition, The CMIP6 historical simulations begin in 1850 and extend to the time near present, which can provide rich opportunities to assess model capability in simulating century timescale climate variability (Flato et al., 2013).

3. Results

3.1. AMO's influence on precipitation over semi-arid regions of the NH

As a multidecadal oscillation, the AMO can regulate climate variability over a long-time scale, so we focus on the linkage between AMO and precipitation over the multidecadal scale. We extract the decadal to multidecadal components of the standardized AMO, since it is characterized primarily by the multidecadal scale (Gan et al., 2019; Huang et al., 2017; Luo et al., 2019; Wu et al., 2011). The filtered AMO index clearly presents a period of more than 60 years (Fig. 1a). Fig. 1b shows uneven spatial distributions of precipitation in the semi-arid regions of the NH. Mean precipitation in the semi-arid regions of North Africa, India, and the southern edge of North America exceeds 500 mm per year, while in the semi-arid regions of mid-latitude Asia, annual precipitation is generally less than 200 mm. In addition, clear dependency on latitude with more precipitation for lower latitudes can be seen in the Eastern Hemisphere. To explore the connection between the precipitation over NH semi-arid regions and AMO, we compared the pattern of regression coefficients between the two with climatological mean precipitation. The patterns of regression coefficients between precipitation and AMO are shown in Fig. 1c. The negative anomalies are mainly

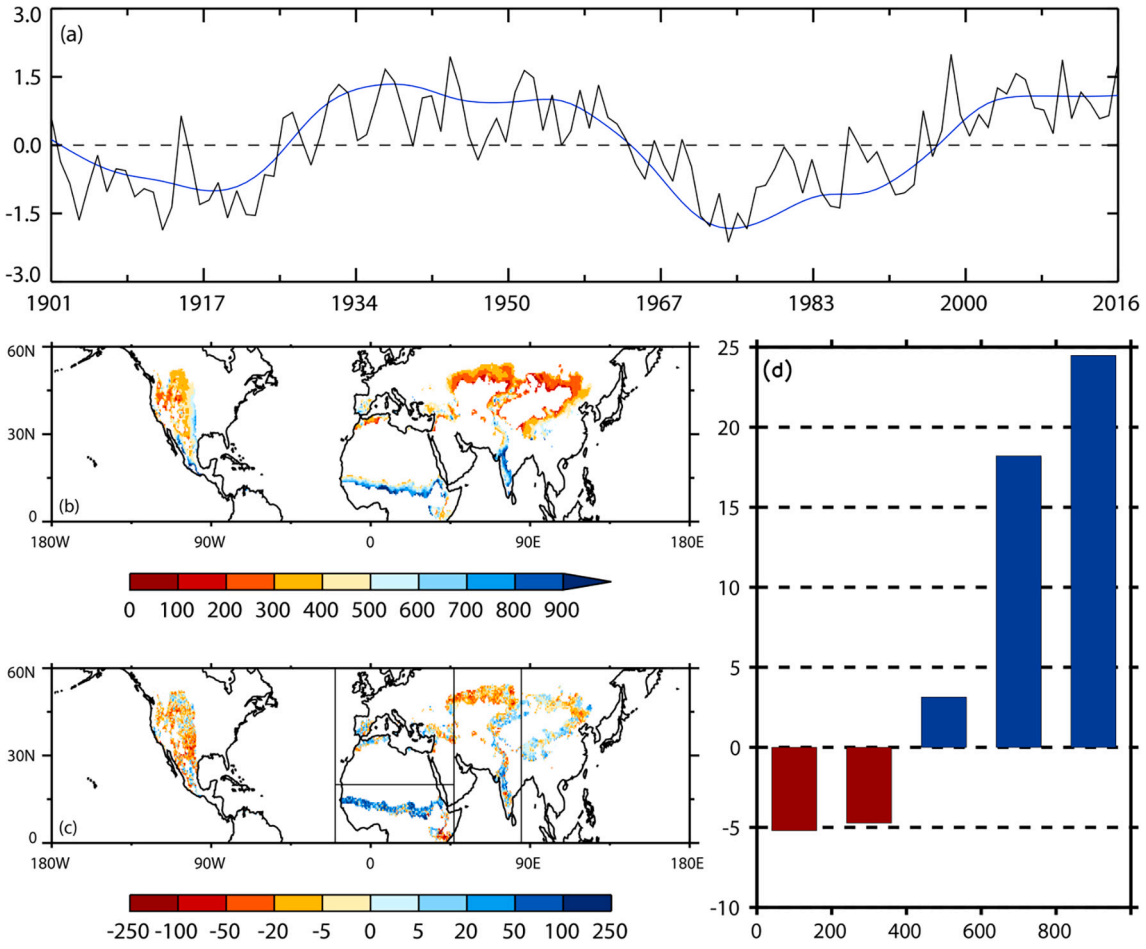

Fig. 1. (a) Time series of AMO index from 1901 to 2016 (normalized). The black curve denotes the unfiltered AMO index, and the blue curve denotes the decadal to multidecadal components of the AMO. (b) Spatial patterns of climatological mean precipitation (units: mm a^{-1}) from 1987 to 2016. (c) regression coefficient (units: mm a^{-1}) between annual mean precipitation and AMO from 1901 to 2016 in the semi-arid regions of the NH. The semi-arid regions are divided into five parts (black lines). (d) Area weighted average regression coefficient (units: mm) between annual mean precipitation and AMO under different semi-arid precipitation (units: mm a^{-1}) areas of the NH. (For interpretation of the references to colour in this figure legend, the reader is referred to the web version of this article.)

concentrated in the semi-arid regions of North America and higher latitudes of the Eastern Hemisphere, while positive anomalies are distributed in lower latitudes of the Eastern Hemisphere. The regression coefficient shows the correlation pattern to the observed climatological mean precipitation. In addition, Fig. 1d shows that the area weighted average regression coefficients between annual mean precipitation and AMO are increased along with local precipitation amount, and are respectively −5.19, −4.72, 3.13, 18.20, 24.48 in the 0 mm −200 mm, 200 mm −400 mm, 400 mm −800 mm and > 800 mm precipitation area. For instance, during the positive phase of the AMO in 1987–2016, the negative anomalies occurred in the regions with annual precipitation below 400 mm, and the positive anomalies were associated with annual precipitation more than 400 mm, which suggests precipitation over the areas with annual precipitation below 400 mm decreased and over the areas with annual precipitation of more than 400 mm increased (Fig. 1d). In particular, the above patterns show better consistency around the Atlantic Ocean. Such patterns indicate that the AMO has exerted a significant influence on the precipitation in NH semi-arid regions.

It is obvious that the AMO index recorded by the instruments used here consists of two cycles during 1901–2016. Based on the cycles, the modern AMO can be divided into two periods: one from 1901 to 1963, and the other from 1964 to 2016 (Fig. 1a). By comparing the relationship between AMO and precipitation in these two periods, we establish a long-term and stable connection between AMO and precipitation, which can provide a better prediction of future precipitation in the semi-arid regions (Sutton and Dong, 2012). Fig. 2 show the spatial distributions of precipitation averaged anomalies (relative to climatological mean) for the positive phases and negative phases of the AMO, which is also demonstrated in CRU TS v. 4.05 data set (Fig. S2). The patterns of precipitation composite for AMO+ (positive AMO phase) and AMO- (negative AMO phase) are in a high degree of consistency between the two periods, especially around the North Atlantic. In the positive phase, the vast majority of the semi-arid regions in North America show decreased rainfall (the reduced value is more than 20 mm) except in some marginal areas (precipitation increased in the northernmost areas), while the semi-arid regions in North Africa present strongly increased precipitation and the variations range from 20 mm −50 mm. During the same phase, more precipitation is distributed in the Iberian Peninsula and Asia Minor Peninsula but the variations are only 10 mm. In the semi-arid regions of Asia, the most significant changes of precipitation in the positive phase are the increased pattern (more than 50 mm) in the subcontinent of India (Fig. 2a and c). An opposite pattern of precipitation variation is found in the negative phases (Fig. 2b and d). The correlation coefficients between AMO and precipitation during the two periods (Fig. S3) are greater than 0.6 or less than −0.6, and pass the 95% significance test, which also suggests the strong connection between AMO and precipitation in the semi-arid regions. Such similar relationship of AMO and semi-arid precipitation between the two periods suggests that similar mechanisms may be responsible for the AMO-

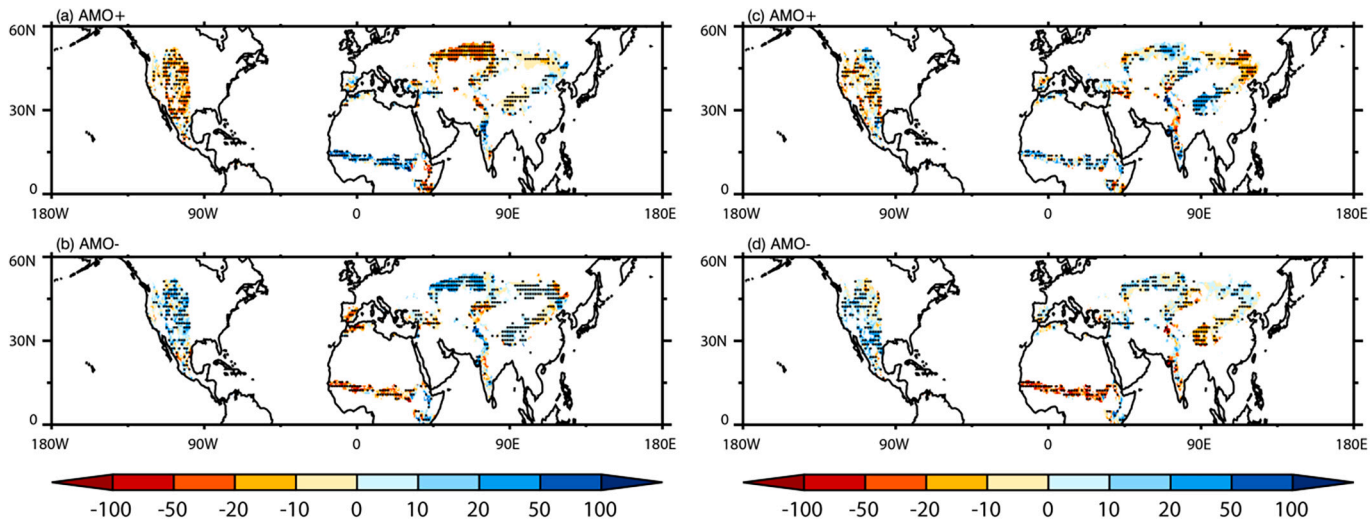

Fig. 2. Precipitation (low-pass-filtered) composite for different phases of the AMO in the semi-arid regions of the NH (units: mm). Panel (a) is in the positive phase during 1901–1963, panel (b) is in the negative phase during 1901–1963, panel (c) is in the positive phase during 1964–2016, and panel (d) is in the negative phase during 1964–2016. Stippling denotes the region with statistical significance at the 95% confidence level based on Student's *t*-test.

modulated precipitation in the semi-arid regions, and similar climate impacts may exist (Sutton and Dong, 2012).

Due to the broad distribution of semi-arid regions in the NH, the effects of the AMO on each region differ (Knight et al., 2006; Sutton and Hodson, 2007). To have a better understanding of the AMO's impacts, we divide the NH semi-arid regions into five parts (Fig. 1c), namely, semi-arid regions in North America, North Africa, Mediterranean, Central Asia and East Asia. In addition, we define the weighted average of precipitation as the precipitation index in each region. The precipitation index is dealt with in the same way as the AMO index to obtain the decadal to multidecadal components. Fig. 3 demonstrates the lead-lag correlation analysis between precipitation and AMO indices. The precipitation index in North America is negatively correlated with the AMO index ($r = -0.711$, $p < 0.01$), but it did not perform well during 1936–1950. The precipitation index in North Africa evolves in accordance with the AMO, with a positive simultaneous correlation ($r = 0.781$, $p < 0.01$). In Mediterranean and Central Asia, the precipitation index is negatively correlated with the AMO index; and the AMO index leads the precipitation index by 13 and 12 years, respectively. However, the AMO index lags the precipitation index by six years in East Asia, and the precipitation index is positively correlated with the AMO index ($r = 0.309$, $p < 0.01$). In summary, we find that the closer to the North Atlantic, the more rapid response of precipitation, and the stronger the relationship between precipitation and AMO. Such relationship can also be checked by CRU TS v. 4.05 data set (figures omitted).

3.2. A mechanism for AMO's influence on precipitation over semi-arid regions of the NH

A key question to be answered is how the AMO only affects the precipitation in the semi-arid regions of the NH. To address this, we explore the geopotential height and wind fields at different levels of the troposphere. The vast majority of the precipitation in NH semi-arid regions is concentrated in summer, which contributes more than ~40% of annual precipitation except Mediterranean (Fig. S4). Considering abundant precipitation in summer, we focus on the mechanism for precipitation changes in this season, which should largely determine the annual precipitation. Besides, according to the results in Section 3.1, the AMO does not play a dominant role in precipitation over the semi-arid regions of Asia, so we mainly explore the mechanism of the semi-arid regions around the North Atlantic.

The AMO's impacts on semi-arid precipitation in North America can be explained by the atmospheric circulation field (Fig. 7). During the positive phase of AMO (Fig. 7a), SST over the subtropical North Atlantic and the eastern subtropical Pacific is about 0.3 °C higher than normal (Fig. S5a), which would excite a low-pressure anomaly over the subtropical North Atlantic, and a low-pressure anomaly centered over the eastern subtropical Pacific (Fig. S6a). In addition, there is an anomalous low pressure over North America (Fig. S6a). These three negative anomaly centers associate three cyclonic circulation anomalies in the lower troposphere (Fig. 4a), as reported in numerical model experiments (Hu and Feng, 2012). The cyclonic circulation anomalies in North America and the North Atlantic intersect over the North American continent (northerly wind anomalies at the west of Atlantic cyclonic circulation and southerly wind anomalies at the east of North American cyclonic circulation converge over the North American continent), causing strong low-level divergence anomalies. The low-level flow field supports the notion that the precipitation in North America will decrease during the positive phase of the AMO. A significant lowering of SLP over North Africa is consistent with a deepening of the heat low in Sahara (Fig. S6a). Such heat low occurs several days before the monsoon onset for the climatological date (Lavaysse et al., 2009; Martin and Thorncroft, 2014), and can greatly modulate the summer monsoon (Pu and Cook, 2012). The anomalous SLP pattern in the semi-arid regions of Sahel will strengthen the monsoon circulation and increase rainfall in summer (Fig. 4a).

During the negative phase of AMO (Fig. 7b), SST over the subtropical North Atlantic and the eastern subtropical Pacific is about 0.3 °C lower than normal (Fig. S5b), which would excite a high-pressure anomaly over the subtropical North Atlantic, and a high-pressure anomaly centered over the eastern subtropical Pacific (Fig. S6b). However, because of the mountainous terrain in western North America, the atmospheric circulation in the negative phase of the AMO does not present the opposite pattern as that in the positive phase of the AMO (Fig. 4b). The high elevation of the Rocky Mountains results in relatively lower summer pressure in western North America (Fig. S6b). The pressure gradient difference favors southerly flow from the Gulf of Mexico going northward, opening a channel for low-level moisture transport from the Gulf of Mexico to the inland of North America and the anticyclonic circulation anomaly over the subtropical North Atlantic override the North American continent which would enhance the southerly flow (Fig. 4b). The warm and wet airmass anomalies converge, resulting in anomalous ascending motion and more rainfall in the semi-arid regions of North America during the negative phase of the AMO. Over North

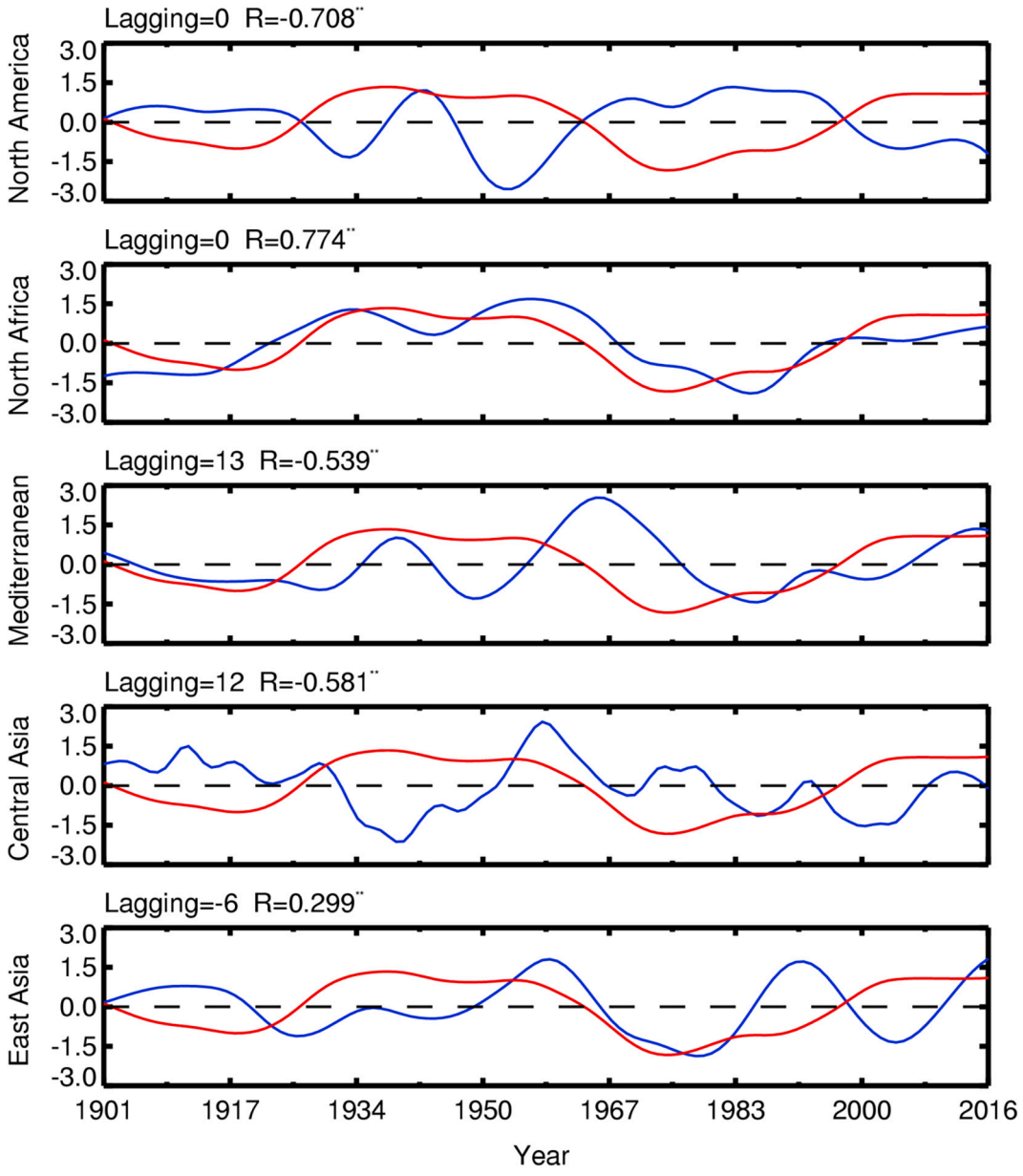

Fig. 3. Lead-lag correlation analysis between regional precipitation index and AMO index. The red line denotes the AMO index, and the blue line denotes the precipitation index. All the correlation coefficients are statistically significant at the 95% confidence level based on Student's t-test. (For interpretation of the references to colour in this figure legend, the reader is referred to the web version of this article.)

Africa and its adjacent ocean areas, an opposite SLP anomaly occurs (Fig. S6b); and there is almost a 180° reversal of wind direction against the positive phase of the AMO. Consequently, the summer monsoon in Sahel is weakened, and the semi-arid regions will have a relatively dry summer in the negative phase of the AMO (Fig. 4b).

The analysis of sectorially averaged omega field reveals that the semi-arid regions in North America have very deep circulation anomalies during different phases of the AMO (Fig. 5). The related strong ascending motion anomalies can reach 200 hPa (Fig. 5a and b). The omega field in the semi-arid regions of North America during the positive phase of the AMO shows that the ascending motion anomalies occur over large areas, but two deep descending motion anomalies occur around 30°N and 45°N, respectively. These anomalous descending motions correspond well with the divergence in the lower troposphere (Figs. 4a and 7a). An opposite flow pattern appears in the negative phase of the AMO (Figs. 5b and 7b). These results highlight the importance of analyzing the upper-level flow field at 200 hPa and seeking an enclosed circulation system that is associated with the lower-level flow field. However, for the semi-arid regions in North Africa, the convection in the vertical wind field caused by the African heat low only reaches 600 hPa, and the strongest center is in the middle of the semi-arid regions during both phases of the AMO (Fig. 5c and d).

Opposite to the anomalous pressure field in the lower troposphere, a broad region of positive geopotential height anomalies appears in the upper atmosphere around the Atlantic Ocean during the positive phase of the AMO (Figs. 6c and 7a). This indicates that the convergence induced by cyclonic circulation anomalies in the lower level causes ascending motion anomalies up to 200 hPa, and then the air masses diverge at 200 hPa. Corresponding to the high-pressure anomalies, two relatively weak anticyclonic circulation anomalies occur over the upper level of the Atlantic Ocean and eastern Pacific Ocean, which manifests the reversed patterns between upper and lower-level troposphere (Figs. 4a and 6c). However, there exists subsidence in the Midwest of North America because the anomalous lower-level divergence generated

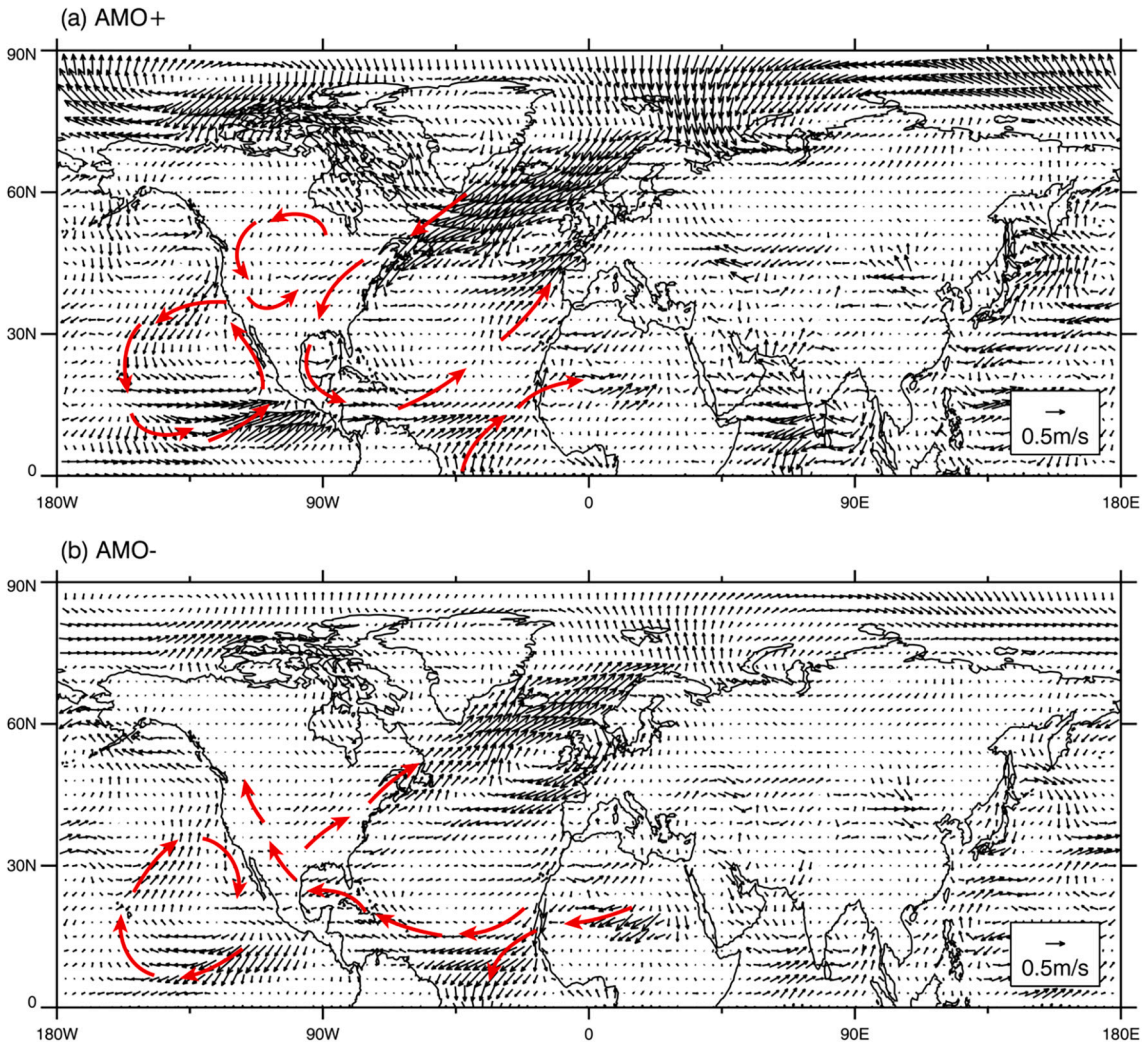

Fig. 4. NH summer surface wind (low-pass-filtered) composite for different phases of AMO during 1964–2016 (units: m s^{-1}). Panel (a) is the positive phase, and panel (b) is the negative phase.

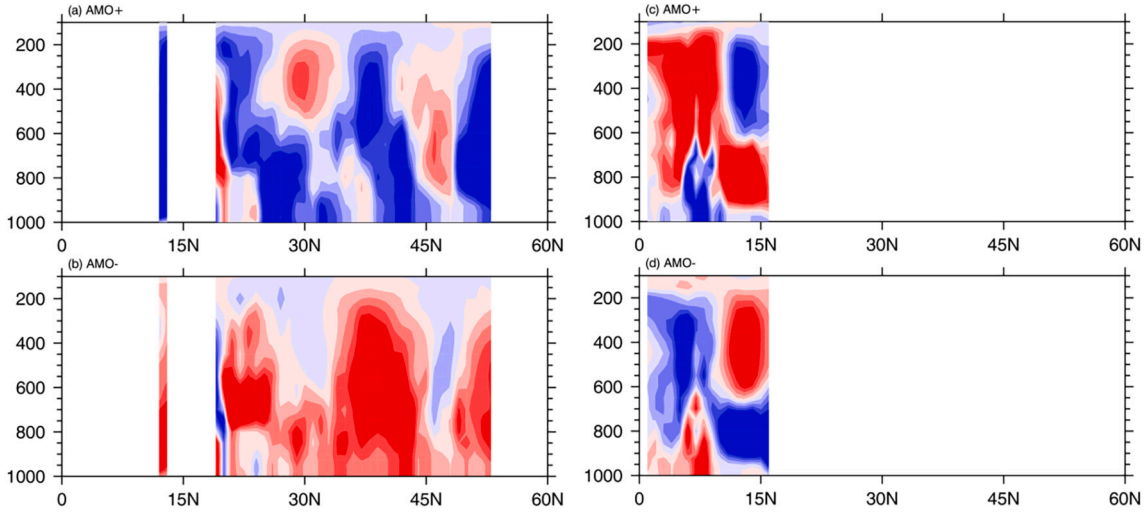

Fig. 5. Sectorially averaged omega (low-pass-filtered; units: Pa s^{-1}) composite for different phases of AMO during 1964–2016 over semi-arid regions over North America (a, b) and North Africa(c, d). Panels (a) and (c) are in the positive phase; and panels (b) and (d) are in the negative phase. The red shading denotes omega greater than 0, indicating downward movement. The blue shading denotes omega less than 0, indicating upward movement. (For interpretation of the references to colour in this figure legend, the reader is referred to the web version of this article.)

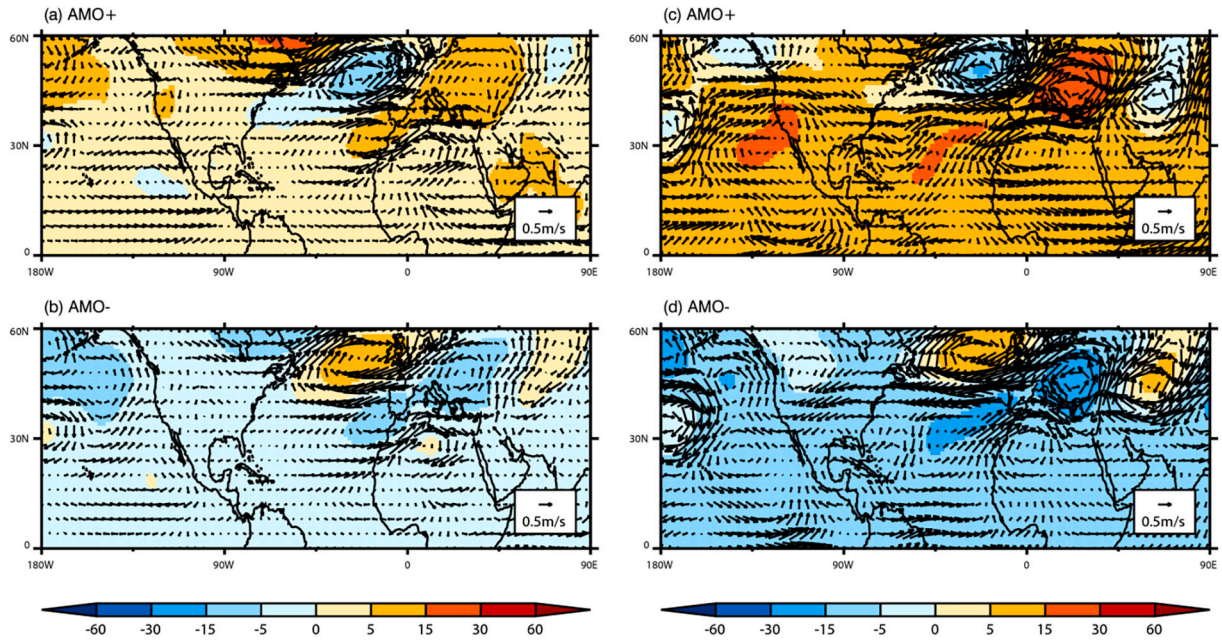

Fig. 6. Circulation anomalies (low-pass-filtered) composite for different phases of AMO during 1964–2016 at 600 hPa (a, b) and 200 hPa (c, d). Panels (a) and (c) are the positive phase; panels (b) and (d) are the negative phase. The shading represents the geopotential height field (units: m), and the arrow represents the wind field (units: m s^{-1}).

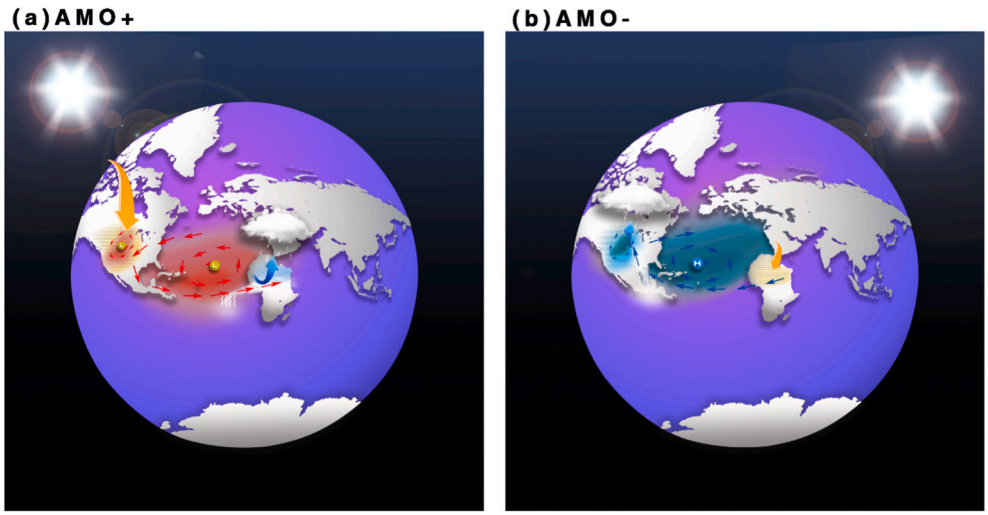

Fig. 7. Schematic sketch for the mechanism of AMO's impacts on precipitation over North America and North Africa. (a) and (b) are in the positive and negative phase of AMO respectively.

by wind field is largely compensated by anomalous upper-level convergence in front of the ridge over the Midwest of North America (Fig. 6c). We find that the fairly stable system favors less rainfall in the semi-arid regions of North America (Fig. 2a and c). For the semi-arid regions in North Africa, the low-pressure anomalies intensify the monsoon, raise the warm and moist air, and increase local precipitation (Fig. 2a and c). Accordingly, the air masses are transported to 600 hPa (Fig. 6a), causing positive geopotential height anomalies. As a result, the divergence anomalies occur at 600 hPa near 15°N behind the ridge (Fig. 7a).

In the negative phase of the AMO (Fig. 7b), the circulation anomalies at 200 hPa over the Atlantic Ocean are generally opposite to those in the positive phase of the AMO, and there is an anticyclonic circulation anomaly over the mid-latitude North American continent (Fig. 6d). The upper troposphere circulation is the result of ascending motion from the lower troposphere. When the air mass is lifted to a certain height, water vapor condenses and forms precipitation. The remaining drier and cooler air mass continues to rise, resulting in an anticyclonic divergence at 200 hPa. The semi-arid regions in North Africa are below the trough at 600 hPa near 15°N (Fig. 6b). A strong convergence behind the trough provides descending mechanism that prevents storm development and encourages negative precipitation anomalies in the semi-arid regions during the negative phase of the AMO (Fig. 2b and d).

3.3. *Predicting the precipitation over semi-arid regions by AMO*

Climate models are useful tools for investigating climate change, so we used 14 CMIP6 models to evaluate their simulation capabilities to AMO. The time series of the AMO index constructed by North Atlantic-averaged SST from observations and models are shown in Fig. 8a. The

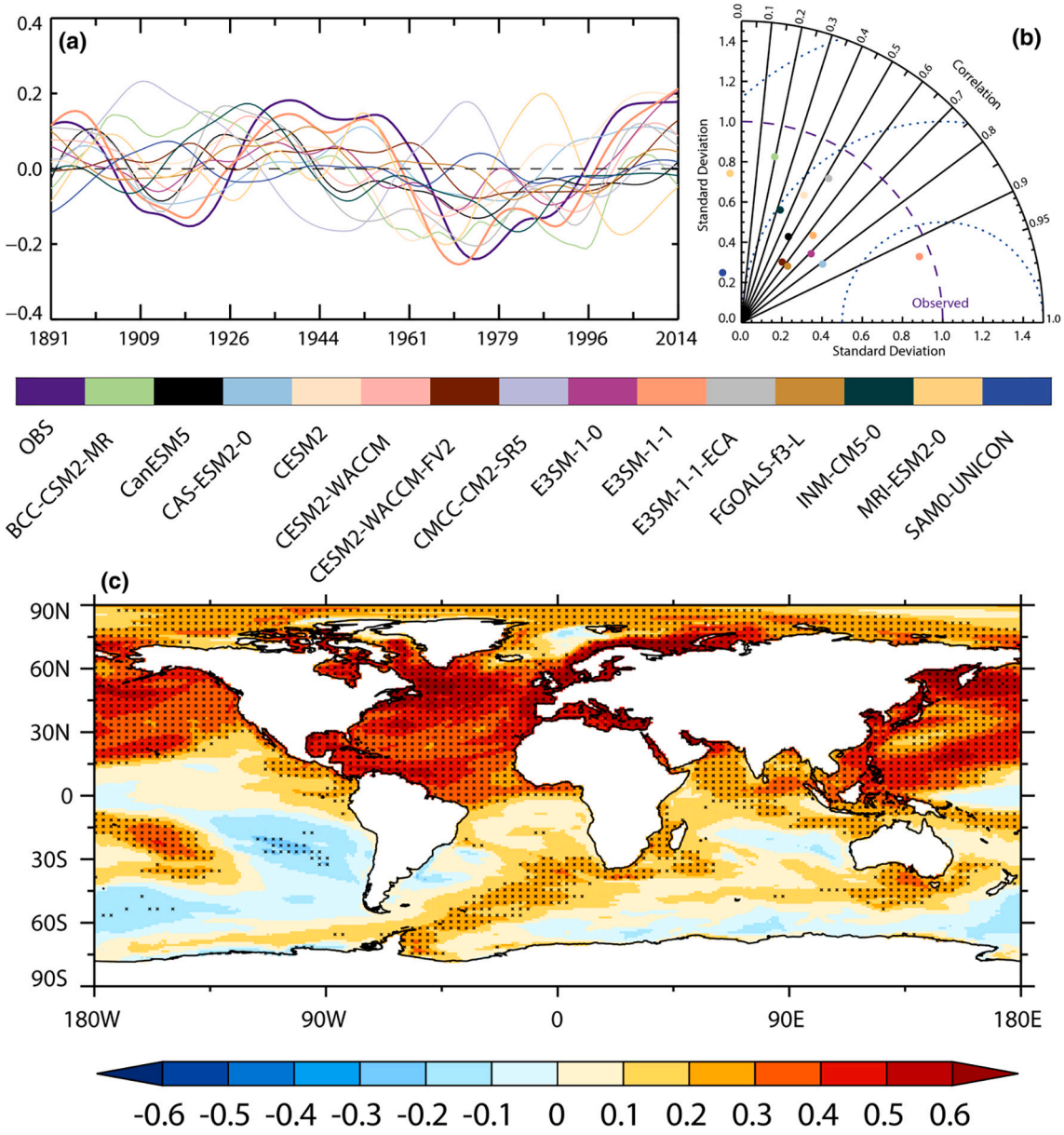

Fig. 8. (a) Time series of the decadal to multidecadal components of AMO in CMIP6 models and observation (units: °C). (b) Taylor diagram of the low-pass-filtered AMO index simulated in the models during the period 1891–2014. (c) Spatial distribution of correlation coefficient between AMO and SST in E3SM 1–1. Stippling denotes the region with statistical significance at the 95% confidence level based on Student's *t*-test.

AMO index in E3SM 1–1 is almost consistent with the observations, which is also presented in the Taylor diagram (Fig. 8b). The correlation coefficient is 0.94 and the ratio of their variances is 0.94, manifesting a high degree of agreement which indicates that E3SM 1–1 can simulate the AMO using both amplitude and phase. Moreover, the results show a high correlation coefficient exists between AMO and SST in E3SM 1–1 over the NH, which is consistent with the observations (Fig. 8c), and implies SST is the key variable in the simulation of multidecadal precipitation in semi-arid regions (García-Serrano et al., 2015; Hatzaki and Wu, 2015; Lyu and Yu, 2017). These results raise hope for some long-term predictability of precipitation over semi-arid regions around the Atlantic, provided that the AMO is correctly represented in coupled ocean-atmosphere models (Peings et al., 2016).

In addition, the AMO's impacts can be roughly presented in E3SM 1–1 when the SST is relatively consistent with observations (Fig. 9). During the positive phase of AMO, precipitation decreased in the southern part of the semi-arid regions of North America and increased in the northern part of the semi-arid regions of North America. Compared with the observations, the wet area expands in the northern part of the region, and the variation in the southern part and the northern part of the semi-arid regions were both more than 20 mm. Precipitation changed slightly (less than 10 mm) in the middle of semi-arid regions. The precipitation change in the semi-arid regions of North Africa is consistent with the observations, but the variation is more uniform, with the precipitation increasing by 20 mm. The relationship between precipitation and AMO in other semi-arid regions is relatively unstable, and this instability is also reflected in the model. This instability is manifested by a large gap between the results obtained by the model and the observations. The precipitation changes in the semi-arid regions of North America and North Africa show opposite patterns when AMO is in the negative phase. By comparing models with observations, we find that the AMO relationship with precipitation can be partially reproduced, especially in areas where the relationship is relatively stable in observations, such as the semi-arid regions over the southern part of

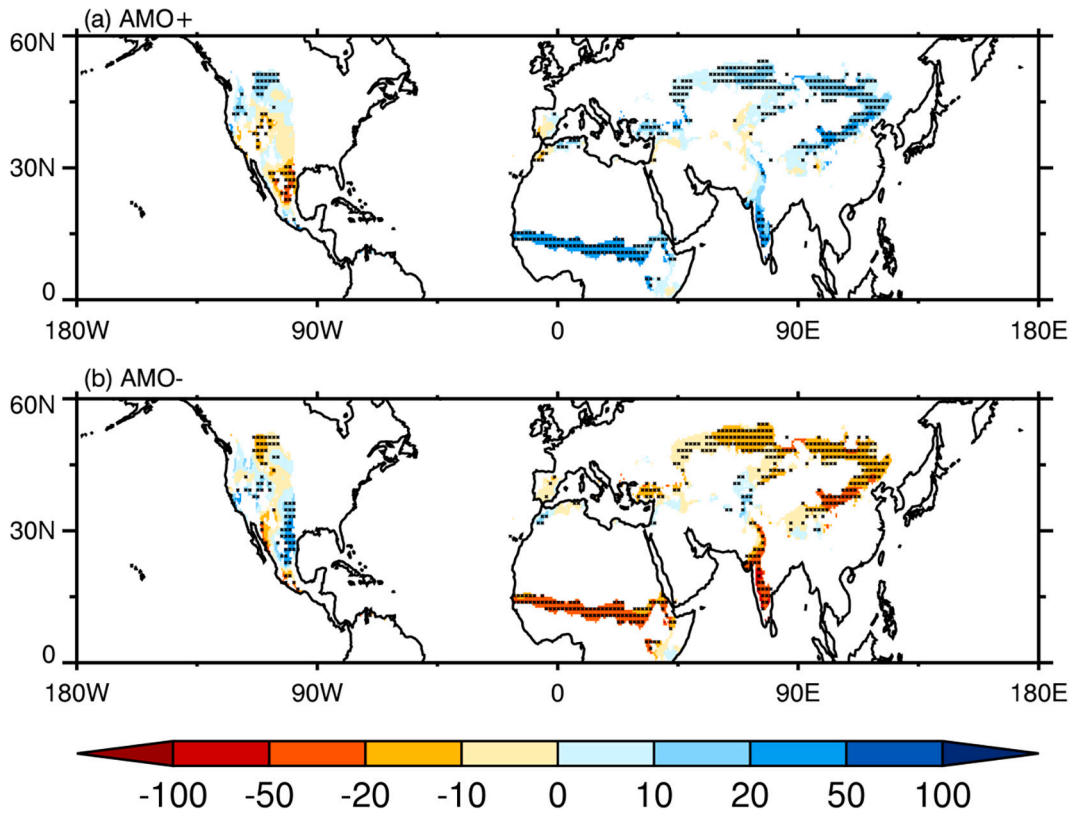

Fig. 9. Precipitation (low-pass filtered) composite for different phases of AMO over the semi-arid regions of NH (units: mm) in E3SM 1–1. Panel (a) is the positive phase, and panel (b) is the negative phase. Stippling denotes the region with statistical significance at the 95% confidence level based on Student's t-test.

North America and the semi-arid regions of North Africa. With the good agreement between observed and simulated AMO in E3SM 1–1, the semi-arid regions will encounter the negative AMO phase (Fig. S7) and experience a different precipitation pattern. According to our prediction, AMO will be in its negative phase in the next decade, precipitation in the southern part of North America will increase by more than 20 mm, and the entire semi-arid region of North Africa could see a decrease in rainfall by more than 20 mm.

4. Conclusions and discussion

Due to the unique environment, the atmospheric stability and circulation in semi-arid regions are different from other areas. In this study, we focused on the relationship between regional precipitation and AMO in the semi-arid regions of the NH. The patterns of regression coefficient between precipitation and AMO are in good correspondence to climatological mean precipitation, particularly over the semi-arid regions near the North Atlantic. Such relationship is specifically manifested as precipitation change, such that rainfall over the areas with annual precipitation below 400 mm decreased and over the areas with annual precipitation of more than 400 mm increased in the semi-arid regions as the AMO underwent a phase transition from a negative phase to a positive phase in the past 30 years. Therefore, the AMO can exert a great influence on multidecadal precipitation variability over large parts of the NH. Both positive phases during 1901–1963 and 1964–2016 demonstrated less precipitation (the reduced value is more than 20 mm) in the semi-arid regions of North America except in some marginal areas (precipitation increased in the northernmost areas), more precipitation (the range from 20 mm −50 mm) in most semi-arid regions of North Africa, and slightly more precipitation in the Iberian Peninsula and Asia Minor Peninsula with only 10 mm of recorded variation. The most significant changes of precipitation in the positive phase are the increased pattern (more than 50 mm) in the subcontinent of India. Roughly opposite patterns occurred in the negative phase of the AMO. This consistency suggests that the AMO maintains a long-term, robust relationship with precipitation in NH semi-arid regions, especially around the North Atlantic sector. The closer to the North Atlantic, the more rapid response of precipitation, and the stronger the relationship between precipitation and AMO.

Such a clear influence of the AMO on precipitation is due to the atmospheric circulation system. In summer, during the positive phase of the AMO, the positive anomalous SST weakened the SLP over the Atlantic and eastern Pacific. The anomalous SLP changed the regional atmospheric activities over the semi-arid regions around the Atlantic. Then, three cyclonic circulation anomalies appeared over North Atlantic, North America, and eastern Pacific. The cyclonic circulation anomalies intersected over the semi-arid regions of North America and caused low-level divergence and the North Atlantic cyclone enhanced the African monsoon, even affecting the precipitation in the semi-arid regions around the Atlantic. A roughly opposite flow field occurs during the negative phase of the AMO. Therefore, the simulation ability of the AMO in a model is the key for the multidecadal prediction of precipitation over semi-arid regions. By comparison, we selected E3SM 1–1 as the best model for reconstructing the AMO. Using it for prediction, AMO will be in the negative phase in the next decade, precipitation in the southern part of North America will increase by more than 20 mm, and the entire semi-arid region of North Africa could see a decrease in rainfall by more than 20 mm.

Declaration of Competing Interest

The authors declare that they have no known competing financial interests or personal relationships that could have appeared to influence the work reported in this paper.

Acknowledgments

This work is supported by National Natural Science Foundation of China (42041004, 41722502 and 41521004), the Strategic Priority Research Program of Chinese Academy of Sciences (Grant No. XDA2006010301), and the Fundamental Research Funds for the Central Universities (lzujbky-2019-kb30). We also thank all the institutions providing data for this research. The precipitation dataset is from GPCC. The AI dataset used in this study is provided by Huang et al. (2020). AMO index and the 20th Century Reanalysis V3 data are provided by the NOAA/OAR/ESRL PSD, Boulder, Colorado, USA, from their website at https://psl.noaa.gov/data/timeseries/AMO/

Appendix A. Supplementary data

Supplementary data to this article can be found online at https://doi.org/10.1016/j.atmosres.2021.105801.

References

Chang, C.P., Wang, Z., Ju, J., Li, T., 2004. On the relationship between western maritime continent monsoon rainfall and ENSO during northern winter. J. Clim. 17 (3), 665–672. https://doi.org/10.1175/1520-0442(2004)017<0665:OTRBWM>2.0.CO;2.

Dai, A., 2011. Drought under global warming: a review. Wiley Interdiscip. Rev. Clim. Chang. 2 (1), 45–65. https://doi.org/10.1002/wcc.81.

Enfield, D.B., Mestas-Nuñez, A.M., Trimble, P.J., 2001. The Atlantic multidecadal oscillation and its relation to rainfall and river flows in the continental US. Geophys. Res. Lett. 28 (10), 2077–2080. https://doi.org/10.1029/2000GL012745.

Eyring, V., Bony, S., Meehl, G.A., Senior, C.A., Stevens, B., Stouffer, R.J., Taylor, K.E., 2016. Overview of the coupled model intercomparison project phase 6 (CMIP6) experimental design and organization. Geosci. Model Dev. 9 (5), 1937–1958. https://doi.org/10.5194/gmd-9-1937-2016.

FAO, 1977. World Map of Desertification. United Nations Conference on Desertification, Nairobi.

Feng, S., Fu, Q., 2013. Expansion of global drylands under a warming climate. Atmos. Chem. Phys. 13 (19), 10081–10094. https://doi.org/10.5194/acp-13-10081-2013.

Flato, G., Marotzke, J., Abiodun, B., Braconnot, P., Chou, S.C., Collins, W., Cox, P., Driouech, F., Emori, S., Eyring, V., Forest, C., Gleckler, P., Guilyardi, E., Jakob, C., Kattsov, V., Reason, C., Rummukainen, M., 2013. Evaluation of climate models. In: Stocker, T.F., Qin, D., Plattner, G.-K., Tignor, M., Allen, S.K., Boschung, J., Nauels, A., Xia, Y., Bex, V., Midgley, P.M. (Eds.), Climate Change 2013: The Physical Science Basis. Contribution of Working Group I to the Fifth Assessment Report of the Intergovernmental Panel on Climate Change. Cambridge University Press, Cambridge, United Kingdom and New York, NY, USA.

Gan, Z., Guan, X., Kong, X., Guo, R., Huang, H., Huang, W., Xu, Y., 2019. The key role of Atlantic Multidecadal Oscillation in minimum temperature over North America during global warming slowdown. Earth Space Sci. 6 (3), 387–397. https://doi.org/10.1029/2018EA000443.

Gao, T., Wang, H.J., Zhou, T., 2017. Changes of extreme precipitation and nonlinear influence of climate variables over monsoon region in China. Atmos. Res. 197 (nov), 379–389. https://doi.org/10.1016/j.atmosres.2017.07.017.

García-Serrano, J., Guemas, V., Doblas-Reyes, F.J., 2015. Added-value from initialization in predictions of Atlantic multi-decadal variability. Clim. Dyn. 44 (9–10), 2539–2555. https://doi.org/10.1007/s00382-014-2370-7.

Gong, D.Y., Shi, P.J., Wang, J.A., 2004. Daily precipitation changes in the semi-arid region over northern China. J. Arid Environ. 59 (4), 771–784. https://doi.org/10.1016/j.jaridenv.2004.02.006.

Gu, G., Adler, R.F., Huffman, G.J., Curtis, S., 2007. Tropical rainfall variability on interannual-to-interdecadal and longer time scales derived from the GPCP monthly product. J. Clim. 20 (15), 4033–4046. https://doi.org/10.1175/JCLI4227.1.

Guan, X., Huang, J., Guo, R., 2017. Changes in aridity in response to the global warming hiatus. J. Meteorol. Res. 31 (1), 117–125. https://doi.org/10.1007/s13351-017-6038-1.

Guan, X., Ma, J., Huang, J., Huang, R., Zhang, L., Ma, Z., 2019. Impact of oceans on climate change in drylands. Sci. China Earth Sci. 62 (6), 891–908. https://doi.org/10.1007/s11430-018-9317-8.

Harris, I., Osborn, T.J., Jones, P., Lister, D., 2020. Version 4 of the CRU TS monthly high-resolution gridded multivariate climate dataset. Sci. Data 7 (1), 1–18. https://doi.org/10.1038/s41597-020-0453-3.

Hatzaki, M., Wu, R., 2015. The South-Eastern Europe winter precipitation variability in relation to the North Atlantic SST. Atmos. Res. 152, 61–68. https://doi.org/10.1016/j.atmosres.2013.10.008.

Hu, Q., Feng, S., 2012. AMO-and ENSO-driven summertime circulation and precipitation variations in North America. J. Clim. 25 (19), 6477–6495. https://doi.org/10.1175/JCLI-D-11-00520.1.

Hu, Q., Feng, S., Oglesby, R.J., 2011. Variations in North American summer precipitation driven by the Atlantic multidecadal oscillation. J. Clim. 24 (21), 5555–5570. https://doi.org/10.1175/2011JCLI4060.1.

Huang, J., Yu, H., Guan, X., Wang, G., Guo, R., 2016. Accelerated dryland expansion under climate change. Nat. Clim. Chang. 6 (2), 166–171. https://doi.org/10.1038/nclimate2837.

Huang, J., Li, Y., Fu, C., Chen, F., Fu, Q., Dai, A., Shinoda, M., Ma, Z., Guo, W., Li, Z., Zhang, L., Liu, Y., Yu, H., He, Y., Xie, Y., Guan, X., Ji, M., Lin, L., Wang, S., Yan, H., Wang, G., 2017. Dryland climate change: recent progress and challenges. Rev. Geophys. 55 (3), 719–778. https://doi.org/10.1002/2016RG000550.

Huang, J., Ma, J., Guan, X., Li, Y., He, Y., 2019. Progress in semi-arid climate change studies in China. Adv. Atmos. Sci. 36 (9), 922–937. https://doi.org/10.1007/s00376-018-8200-9.

Huang, J., Yu, H., Han, D., Zhang, G., Wei, Y., Huang, J., An, L., Liu, X., Ren, Y., 2020. Declines in global ecological security under climate change. Ecol. Indic. 117, 106651. https://doi.org/10.1016/j.ecolind.2020.106651.

Joshi, M.K., Ha, K.J., 2019. Fidelity of CMIP5-simulated teleconnection between Atlantic multidecadal oscillation and Indian summer monsoon rainfall. Clim. Dyn. 52 (7), 4157–4176. https://doi.org/10.1007/s00382-018-4376-z.

Kerr, R.A., 2000. A North Atlantic climate pacemaker for the centuries. Science 288 (5473), 1984–1985. https://doi.org/10.1126/science.288.5473.1984.

Kim, J.W., Yeh, S.W., Chang, E.C., 2014. Combined effect of El Niño-Southern Oscillation and Pacific decadal oscillation on the East Asian winter monsoon. Clim. Dyn. 42 (3–4), 957–971. https://doi.org/10.1007/s00382-013-1730-z.

Kitzberger, T., Brown, P.M., Heyerdahl, E.K., Swetnam, T.W., Veblen, T.T., 2007. Contingent Pacific–Atlantic Ocean influence on multicentury wildfire synchrony over western North America. Proc. Natl. Acad. Sci. U. S. A. 104 (2), 543–548. https://doi.org/10.1073/pnas.0606078104.

Knight, J.R., Folland, C.K., Scaife, A.A., 2006. Climate impacts of the Atlantic multidecadal oscillation. Geophys. Res. Lett. 33 (17) https://doi.org/10.1029/2006GL026242.

Kong, X., Guan, X., Cao, C., Zhang, T., Shen, L., Gan, Z., Ma, J., Huang, H., 2019. Decadal change in soil moisture over East Asia in response to a decade-long warming hiatus. J. Geophys. Res. Atmos. 124 (15), 8619–8630. https://doi.org/10.1029/2019JD030294.

Lavaysse, C., Flamant, C., Janicot, S., Parker, D.J., Lafore, J.P., Sultan, B., Pelon, J., 2009. Seasonal evolution of the West African heat low: a climatological perspective. Clim. Dyn. 33 (2–3), 313–330. https://doi.org/10.1007/s00382-009-0553-4.

Luo, W., Guan, X., Xie, Y., Liu, J., Zhou, Y., Zhang, B., 2019. The key role of decadal modulated oscillation in recent cold phase. Int. J. Climatol. 39 (15), 5761–5770. https://doi.org/10.1002/joc.6186.

Lyu, K., Yu, J.Y., 2017. Climate impacts of the Atlantic multidecadal oscillation simulated in the CMIP5 models: a re-evaluation based on a revised index. Geophys. Res. Lett. 44 (8), 3867–3876. https://doi.org/10.1002/2017GL072681.

Mantua, N.J., Hare, S.R., Zhang, Y., Wallace, J.M., Francis, R.C., 1997. A Pacific interdecadal climate oscillation with impacts on salmon production. Bull. Am. Meteorol. Soc. 78 (6), 1069–1080. https://doi.org/10.1175/1520-0477(1997)078<1069:APICOW>2.0.CO;2.

Martin, E.R., Thorncroft, C.D., 2014. The impact of the AMO on the West African monsoon annual cycle. Q. J. R. Meteorol. Soc. 140 (678), 31–46. https://doi.org/10.1002/qj.2107.

McCabe, G.J., Palecki, M.A., Betancourt, J.L., 2004. Pacific and Atlantic Ocean influences on multidecadal drought frequency in the United States. Proc. Natl. Acad. Sci. U. S. A. 101 (12), 4136–4141. https://doi.org/10.1073/pnas.0306738101.

McPhaden, M.J., Zebiak, S.E., Glantz, M.H., 2006. ENSO as an integrating concept in earth science. Science. 314 (5806), 1740–1745. https://doi.org/10.1126/science.1132588.

Miao, L., Li, S., Zhang, F., Chen, T., Shan, Y., Zhang, Y., 2020. Future drought in the dry lands of Asia under the 1.5 and 2.0 C warming scenarios. Earth's Future 8 (6). https://doi.org/10.1029/2019EF001337 e2019EF001337.

Middleton, N., Thomas, D., 1997. World Atlas of Desertification. Oxford Univ. Press.

Mo, K.C., Schemm, J.K.E., Yoo, S.H., 2009. Influence of ENSO and the Atlantic multidecadal oscillation on drought over the United States. J. Clim. 22 (22), 5962–5982. https://doi.org/10.1175/2009JCLI2966.1.

Mochizuki, T., Ishii, M., Kimoto, M., Chikamoto, Y., Watanabe, M., Nozawa, T., Sakamoto, T., Shiogama, H., Awaji, T., Sugiura, N., Toyoda, T., Yasunaka, S., Tatebe, H., Mori, M., 2010. Pacific decadal oscillation hindcasts relevant to near-term climate prediction. Proc. Natl. Acad. Sci. U. S. A. 107 (5), 1833–1837. https://doi.org/10.1073/pnas.0906531107.

Peings, Y., Simpkins, G., Magnusdottir, G., 2016. Multidecadal fluctuations of the North Atlantic Ocean and feedback on the winter climate in CMIP5 control simulations. J. Geophys. Res. Atmos. 121 (6), 2571–2592. https://doi.org/10.1002/2015JD024107.

Pu, B., Cook, K.H., 2012. Role of the West African westerly jet in Sahel rainfall variations. J. Clim. 25 (8), 2880–2896. https://doi.org/10.1175/JCLI-D-11-00394.1.

Qian, C., Zhou, T., 2014. Multidecadal variability of North China aridity and its relationship to PDO during 1900–2010. J. Clim. 27 (3), 1210–1222. https://doi.org/10.1175/JCLI-D-13-00235.1.

Ropelewski, C.F., Halpert, M.S., 1987. Global and regional scale precipitation patterns associated with the El Niño/Southern Oscillation. Mon. Weather Rev. 115 (8), 1606–1626. https://doi.org/10.1175/1520-0493(1987)115<1606:GARSPP>2.0.CO;2.

Schlesinger, M.E., Ramankutty, N., 1994. An oscillation in the global climate system of period 65–70 years. Nature. 367 (6465), 723–726. https://doi.org/10.1038/367723a0.

Schneider, U., Becker, A., Finger, P., Meyer-Christoffer, A., Ziese, M., Rudolf, B., 2014. GPCC's new land surface precipitation climatology based on quality-controlled in situ data and its role in quantifying the global water cycle. Theor. Appl. Climatol. 115 (1), 15–40. https://doi.org/10.1007/s00704-013-0860-x.

Scholes, R.J., 2020. The future of semi-arid regions: a weak fabric unravels. Climate 8 (3), 43. https://doi.org/10.3390/cli8030043.
Sutton, R.T., Dong, B., 2012. Atlantic Ocean influence on a shift in European climate in the 1990s. Nat. Geosci. 5 (11), 788–792. https://doi.org/10.1038/ngeo1595.
Sutton, R.T., Hodson, D.L., 2007. Climate response to basin-scale warming and cooling of the North Atlantic Ocean. J. Clim. 20 (5), 891–907. https://doi.org/10.1175/JCLI4038.1.
Ting, M., Kushnir, Y., Seager, R., Li, C., 2011. Robust features of Atlantic multi-decadal variability and its climate impacts. Geophys. Res. Lett. 38 (17) https://doi.org/10.1029/2011GL048712.
Wu, Z., Huang, N.E., 2009. Ensemble empirical mode decomposition: a noise-assisted data analysis method. Adv. Adapt. Data Anal. 1 (01), 1–41. https://doi.org/10.1142/S1793536909000047.
Wu, Z., Huang, N.E., Wallace, J.M., Smoliak, B.V., Chen, X., 2011. On the time-varying trend in global-mean surface temperature. Clim. Dyn. 37 (3), 759–773. https://doi.org/10.1007/s00382-011-1128-8.
Wu, B., Lin, X., Yu, L., 2020. North Pacific subtropical mode water is controlled by the Atlantic Multidecadal Variability. Nat. Clim. Chang. 10 (3), 238–243. https://doi.org/10.1038/s41558-020-0692-5.
Wyatt, M.G., Kravtsov, S., Tsonis, A.A., 2012. Atlantic multidecadal oscillation and Northern Hemisphere's climate variability. Clim. Dyn. 38 (5), 929–949. https://doi.org/10.1007/s00382-011-1071-8.
Xie, Y., Huang, J., Ming, Y., 2019. Robust regional warming amplifications directly following the anthropogenic emission. Earth's Future 7 (4), 363–369. https://doi.org/10.1029/2018EF001068.
Zhang, F., Wang, G., 2018. Effect of irrigation-induced densification on the post-failure behavior of loess flowslides occurring on the Heifangtai area, Gansu, China. Eng. Geol. 236, 111–118. https://doi.org/10.1016/j.enggeo.2017.07.010.